Downloaded from jnm.snmjournals.org by on March 12, 2017. For personal use only.

Quantitative Assessment of Hypoxia Kinetic Models by a Cross-Study of Dynamic ^{18}F-FAZA and ^{15}O-H_2O in Patients with Head and Neck Tumors

Kuangyu Shi[1], Michael Souvatzoglou[2], Sabrina T. Astner[1], Peter Vaupel[1], Fridtjof Nüsslin[1], Jan J. Wilkens[1], and Sibylle I. Ziegler[2]

[1]*Department of Radiotherapy and Radiooncology, Klinikum rechts der Isar, Technische Universität München, Munich, Germany; and* [2]*Department of Nuclear Medicine, Klinikum rechts der Isar, Technische Universität München, Munich, Germany*

Several kinetic models have been proposed to assess the underlying oxygenation status behind hypoxia tracer uptake and have shown advantages, compared with static analysis, in discriminating hypoxic regions. However, the quantitative assessment of mathematic models that take into consideration clinical applications and their biologic nature is still challenging. We performed a feasibility study to assess hypoxia kinetic models using voxelwise cross-analysis between the uptake of the perfusion tracer ^{15}O-H_2O and the hypoxia tracer ^{18}F-fluoroazomycin arabinoside (^{18}F-FAZA). **Methods:** Five patients with advanced head and neck cancer were included. For each patient, dynamic sequences of ^{15}O-H_2O for 5 min and ^{18}F-FAZA for 60 min were acquired consecutively after injections of approximately 1 GBq and 300 MBq of each tracer, respectively. The compartment model, Thorwarth model, Patlak plot, Logan plot, and Cho model were applied to model the process of tracer transport and accumulation under hypoxic conditions. The standard 1-tissue-compartment model was used to compute a perfusion map for each patient. The hypoxia kinetic models were based on the assumption of a positive correlation between tracer delivery and perfusion and a negative (inverse) correlation between tracer accumulation (hypoxia) and perfusion. **Results:** Positive correlations between tracer delivery and perfusion were observed for the Thorwarth and Cho models in all patients and for the reversible and irreversible 2-compartment models in 4 patients. Negative correlations between tracer accumulation and perfusion were observed for the reversible 2-compartment model in all patients and for the irreversible 2-compartment model and Cho model in 4 patients. When applied to normal skeletal muscle, the smallest correlation variance over all 5 patients was observed for the reversible 2-compartment model. **Conclusion:** Hypoxia kinetic modeling delivers different information from static measurements. Different models generate different results for the same patient, and they even can lead to opposite physiologic interpretations. On the basis of our assessment of physiologic precision and robustness, the reversible 2-compartment model corresponds better to the expectations of our assumptions than the other investigated models.

Key Words: kinetic modeling; tumor hypoxia; tumor perfusion; PET; head and neck tumor

J Nucl Med 2010; 51:1386–1394
DOI: 10.2967/jnumed.109.074336

Kinetic modeling is an important method to assess the underlying physiology behind tracer uptake in molecular imaging (*1*). Four-dimensional spatial–temporal images were acquired to observe the behavior of the radiotracer in the region of study, and estimations of quantitative biologic parameters can be achieved by fitting a mathematic model to the time–activity curve of a region of interest or a certain voxel. Compartment models define physiologically different pools of tracer substance as compartments and set up the relationship between these compartments using linear differential equations (*1,2*). Reference tissue models were developed to avoid blood sampling by selecting a region without specific binding of the ligand (*3*). Linearization can be applied to compartment models leading to graphical models (*4,5*), which assume an equilibrium state of the tracer and use linear regression to identify tracer kinetics.

Although there are many well-developed models that cover a broad range of applications, the performance of these models depends on the precision and robustness of both physiologic description and mathematic capability. Understanding the merits and limitations of the different models is important (*6*). The models can be evaluated using a validated gold standard such as microsphere-based measurement for myocardial blood flow models (*6*) and blood sampling for reference tissue models (*7*). Mathematic performance of the models can be assessed using computational simulations (*8–10*).

Received Dec. 23, 2009; revision accepted Jun. 3, 2010.
For correspondence or reprints contact: Kuangyu Shi, Department of Radiotherapy and Radiooncology, Klinikum rechts der Isar, Technische Universität München, Ismaningerstrasse 22, 81675 Munich, Germany.
E-mail: shi@lrz.tum.de
COPYRIGHT © 2010 by the Society of Nuclear Medicine, Inc.

Downloaded from jnm.snmjournals.org by on March 12, 2017. For personal use only.

Tumor hypoxia is considered a main resistance factor of standard radiotherapy and some chemotherapy. It is characterized by an oxygen tension below a certain level (*11*), which can be measured with the Eppendorf polarographic system (*12*). Although the electrode oximetry is widely accepted as a gold standard for hypoxia detection, it is limited by its invasiveness and is feasible only for easily accessible tumors. Various indirect strategies have been proposed to detect the tumor oxygen status noninvasively (e.g., with PET) (*13*). Several hypoxia-specific tracers have been proposed for tumor hypoxia imaging, such as ^{18}F-fluoromisonidazole (^{18}F-FMISO) (*14,15*), ^{18}F-fluoroerythronitroimidazole (*16*), and $^{60/61/64}$Cu-diacetyl-bis(N^4-methylthiosemicarbazone) (*17*). ^{18}F-fluoroazomycin arabinoside (^{18}F-FAZA) is a marker that accumulates quickly in cells under hypoxic conditions (*18,19*).

In practice, hypoxia tracers diffuse over long distances before reaching hypoxic cells, and the characteristic diffusion time varies for different tumor cells (*20*); thus, a static evaluation is not sufficient to discriminate hypoxia from the background (*21*). In contrast, kinetic modeling is able to assess the cellular reaction rate of the tracer accumulation and thus is potentially more reliable for hypoxia assessment. Casciari et al. attempted using a 4-compartment model with 8 free parameters to determine the cellular reaction rate of ^{18}F-FMISO (*22*). A certain number of parameters usually need to be fixed in real applications. Thorwarth et al. proposed a specific model to identify the tumor oxygen status by decomposing the time–activity curve into perfusion, diffusion, and hypoxia-induced retention components based on the 2-compartment model (*21*). Recently, Cho et al. proposed an empiric model that assessed hypoxia by the slope of the late phase of dynamic activities (*23*).

Although these models have been applied to hypoxia, the behavior of the models in regard to oxygen status is generally not clear. Immunohistologic studies with pimonidazole as a hypoxia marker were used as a reference to compare with static hypoxia tracer uptake (*24,25*) and the modeling results of the Cho model (*23*) in preclinical studies. Voxelwise correlations between pimonidazole intensity and ^{18}F-FMISO counts were assessed in tumor regions (*25*). Although a good positive correlation was reported, the similar accumulation mechanisms between pimonidazole and ^{18}F-FMISO make it difficult to interpret the correlation for the assessment. In addition, such comparison is usually difficult for clinical studies. Thus, it is still challenging to evaluate different hypoxia models with regard to the clinical relevance.

The correlation between blood supply and oxygen status has been analyzed using specific PET tracers for hypoxia and perfusion (*26,27*). In this study, we focused on the application of kinetic models to tumor hypoxia and performed a feasibility study based on a cross-analysis of the uptake of the perfusion tracer ^{15}O-H_2O and the hypoxia tracer ^{18}F-FAZA to evaluate these models.

MATERIALS AND METHODS

Patient Data

Five patients, as shown in Table 1, with locally advanced squamous cell head and neck cancer were investigated. Before the PET study, all patients underwent CT or MRI. The study protocol was approved by the ethics committee of the Technische Universität München and was tolerated well by the patients.

Patients were positioned supine on a multiring whole-body PET scanner (ECAT HR+; CTI/Siemens) and immobilized with individually customized 3-point-fixation thermoplastic masks during the whole study for 75–80 min. Approximately 1 GBq of ^{15}O-H_2O was injected intravenously, and dynamic images were acquired for 5 min with the following protocol: 12 frames × 5, 6 × 10, and 6 × 30 s. Arterial blood samples (*9–17*) were taken during the scanning. At 10–15 min after the ^{15}O-H_2O study, dynamic data were acquired for 1 h after an intravenous injection of around 300 MBq of ^{18}F-FAZA using the following protocol: 12 frames × 10, 6 × 30, 2 × 150, 4 × 300, and 3 × 600 s. Meanwhile, an additional 21–34 venous blood samples were acquired for each patient.

The images were obtained in 2-dimensional mode and reconstructed using a filtered backprojection algorithm with the Hanning filter at a cutoff frequency of 0.4 cycle/pixel. Attenuation correction was performed using a transmission scan with 3 rotating ^{68}Ge rod sources. Additionally, all measurements were corrected for physical decay, random counts, and dead time. The voxel size of the reconstructed images was 4.29 × 4.29 × 2.425 mm. A gaussian filter of 8 × 8 × 6 mm was applied to the PET data before further analysis.

The tumors were contoured manually on the CT or MR images using the BrainLab iPlan 4.0 system (BrainLab). The CT or MR images, which were obtained without using the immobilization mask, were coregistered with the summed images of all the temporal frames of the ^{18}F-FAZA PET data for each patient using PMOD software (version 3.0; PMOD Technologies) based on mutual information. The accuracy of the registration was proven by a physician.

Model Assessment Criteria

Besides limited extravascular diffusion, the main cause for the development of hypoxia is a decreased supply of oxygen, which is strongly related to perfusion within a tumor (*11*). On the basis of this knowledge, tumor cells are more likely hypoxic when perfusion is low than when perfusion is high. We used this special relationship between hypoxia and perfusion to evaluate various kinetic models in patients with large tumors. In particular, we hypothesized that the correlation between tracer delivery and perfusion was positive and the correlation between hypoxia and perfusion was negative (inverse).

Furthermore, we assumed the following for physiologic robustness assessment: the correlation of underlying physiologic characteristics for normal muscle is relatively consistent.

On the basis of this assumption, the resulting correlation between ^{18}F-FAZA and ^{15}O-H_2O should behave similarly for different patients. The SD σ of the correlation coefficients for all patients was computed and compared between each model. The model, which results in low σ, is expected to be more physiologically robust.

Static Analysis

A voxelwise correlation of the static uptake between ^{18}F-FAZA (at 1 h after injection) and ^{15}O-H_2O (at 40–70 s after injection) is

Downloaded from jnm.snmjournals.org by on March 12, 2017. For personal use only.

TABLE 1. Patient Characteristics and Voxelwise Correlations Between Static Uptake of ^{18}F-FAZA (at 1 Hour After Injection) and ^{15}O-H_2O (at 40–70 Seconds After Injection) in Tumor Region

Patient no.	Sex	Age (y)	Tumor location	Tumor volume (cm^3)	*r*
1	M	44	Oropharynx/hypopharynx	48.83	0.517
2	M	48	Oropharynx	75.30	0.431
3	M	49	Nasopharynx	111.85	0.272
4	F	61	Tonsillar fossa	25.51	0.445
5	M	56	Base of tongue	256.29	0.340

shown in Table 1. In this study, we use the Pearson correlation coefficient *r* as the index for the correlation of 2 datasets. The value of this coefficient ranges from −1.0 to 1.0. The correlation type is described by the sign of the coefficient, and the strength of the correlation is represented by the magnitude of the coefficient.

Input Function

To construct a suitable input function for kinetic modeling, both image-based carotid artery selection (*28*) and blood sampling of arterial or venous blood were considered. Blood sampling was corrected for delay and then used for the correction of an image-derived input function. We took the peak part of the input function from the image-based method and the rest from blood samples. After that, a 3-parameter exponential model (Eq. 1) was applied to fit the corrected raw input data (*29*):

$$C_{IN}(t) = (A_1 t - A_2 - A_3)e^{L_1 t} + A_2 e^{L_2 t} + A_3 e^{L_3 t}, \qquad \text{Eq. 1}$$

where $C_{IN}(t)$ is the arterial input function. A_1, A_2, and A_3 and L_1, L_2, and L_3 are parameters to fit and represent the magnitudes and spectra, respectively, of the exponential functions.

One example of the fitted blood input function for our computation is shown in Figure 1, together with the averaged time–activity curves of whole tumors and in the musculature of the neck region (behind the cervical spine).

Dynamic ^{15}O-H_2O Modeling

The left half of Figure 2 illustrates the transport mechanism of ^{15}O-H_2O. It is a freely diffusible tracer, which passes through the blood vessel walls rapidly and quickly diffuses through the interstitial and intracellular space. During this process, ^{15}O-H_2O is inert and thus not metabolized. The 1-compartment model (*30*) was applied, which assumes a compartment of extravascular space in addition to the blood compartment (intravascular space). The linear relationship between the blood compartment and the tissue compartment is described in the following equation:

$$\frac{dC_D(t)}{dt} = K_1 C_{IN}(t) - k_2 C_D(t), \qquad \text{Eq. 2}$$

where $C_D(t)$ is the concentration of free ligands in the interstitial and intracellular space and K_1 is a measured perfusion parameter that equals the product of blood flow and extraction.

Dynamic ^{18}F-FAZA PET Modeling

The right half of Figure 2 illustrates the transport mechanisms of ^{18}F-FAZA. It is a relatively large molecule, which diffuses slowly through capillary walls and in the interstitium. Once it reaches hypoxic areas, ^{18}F-FAZA is trapped in the intracellular space by oxygen reduction of the 2-nitroimidazoles. To demonstrate this dynamic process, several models that have been used to analyze tumor hypoxia were applied, including the compartment model (*22*), Patlak plot (*31*), Logan plot (*27*), Thorwarth model (*21*), and Cho model (*23*).

2-Tissue-Compartment Model. The high number of free parameters in the 4-compartment model (*22*) makes voxelwise fitting difficult. For this reason, we applied the standard 2-tissue-compartment model (*1*) to model the process of ^{18}F-FAZA delivery and accumulation.

The 2-tissue-compartment model assumes 2 compartments in the tissue space. The first compartment is for the free ^{18}F-FAZA concentration $C_D(t)$ in the interstitial space and intracellular space, and the second is for the trapped ^{18}F-FAZA concentration $C_A(t)$ in the intracellular space. K_1 stands for the rate of diffusion from plasma to tissue and k_3 for the tracer accumulation rate. k_2 and k_4 are the rate constants representing the transport rate from interstitium to plasma and the dissociation rate of the trapped ligands, respectively.

Linear differential equations were used to model the relationships between these compartments considering diffusion only:

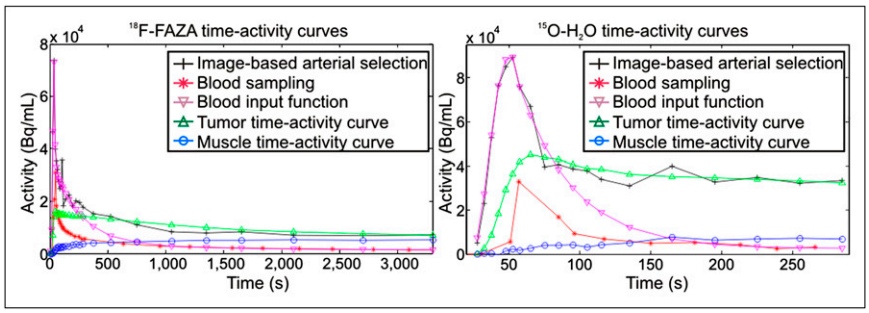

FIGURE 1. Blood input curves and time–activity curves of whole tumor region and 1 normal muscle region for patient 2.

Downloaded from jnm.snmjournals.org by on March 12, 2017. For personal use only.

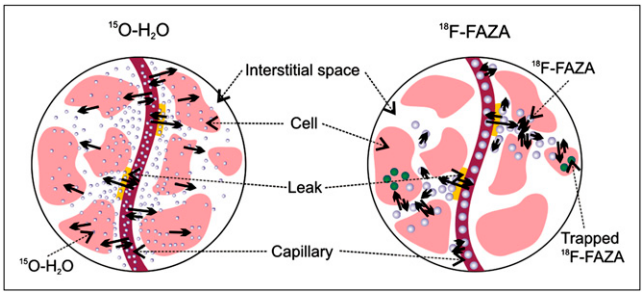

FIGURE 2. Illustration of different transport mechanisms between ^{15}O-H$_2$O and ^{18}F-FAZA.

$$\frac{dC_D(t)}{dt} = K_1 C_{IN}(t) - (k_2 + k_3) C_D(t) + k_4 C_A(t)$$
$$\frac{dC_A(t)}{dt} = k_3 C_A(t) - k_4 C_A(t). \qquad \text{Eq. 3}$$

In addition, we took into consideration the irreversible version of the 2-tissue-compartment model, where k_4 is set to 0.

Thorwarth Model. The Thorwarth model is derived from the irreversible 2-tissue-compartment model and is dedicated to hypoxia modeling (*21*). It decomposes the measured time–activity curve $C_T(t)$ into perfusion, diffusion, and retention curves. Here, w_0, w_D, and w_A are the corresponding weights of each component according to the following equation:

$$C_T(t) = w_0 C_{IN}(t) + w_D C_D(t) + w_A C_A(t)$$
$$C_D(t) = \int_0^t e^{-\tilde{k_3}(t-\tau)} C_{IN}(t) d\tau \qquad \text{Eq. 4}$$
$$C_A(t) = \int_0^t (1 - e^{-\tilde{k_3}(t-\tau)}) C_{IN}(t) d\tau$$

where $\tilde{k_3}$ is the modified accumulation rate constant.

To compare the Thorwarth model under the same condition as the other models, we used the same input function instead of using the reference tissue originally proposed by this model.

Graphical Models. The Patlak model (*4*) is a linearization of the irreversible 2-compartment model, which fits the equation:

$$\frac{C_T(t)}{C_{IN}(t)} = \text{slope} \frac{\int_0^t C_{IN}(\tau) d\tau}{C_{IN}(t)} + \text{intercept}, \qquad \text{Eq. 5}$$

in equilibrium states. Here, slope represents the trapping rate of the tracer in the tissue.

The Logan model (*5*) is a linearization of the reversible 2-compartment model, which fits the equation:

$$\frac{\int_0^t C_T(\tau) d\tau}{C_T(t)} = DV \frac{\int_0^t C_{IN}(\tau) d\tau}{C_T(t)} - \frac{1}{K_2}, \qquad \text{Eq. 6}$$

in equilibrium states. Here the distribution volume *DV* is an index of the metabolic rate of the ligand.

Cho Model. The 2-tissue-compartment, Thorwarth, and graphical models require correct input of blood activity. However, it is difficult to acquire precise information for blood activity. Cho et al. assumed that the retention slope of the last phase of the dynamic scan is a key factor in determining tumor hypoxia and proposed an empiric model (*23*). This model extracts the tracer delivery index, "early," by averaging the activities in the first frames. The tracer accumulation index, "late," is determined from the slope of a straight-line fitting of the last frames. Considering an acquisition time of 1 h for our ^{18}F-FAZA study, we set the first 4 min to be the early phase and the last 40 min to be the late phase.

Voxelwise Model Assessment

Voxelwise computing was performed for each investigated kinetic model, and the correlation of the hypoxia kinetic features and water perfusion was compared voxel by voxel for each patient (Fig. 3).

In addition to cross-analysis in tumor regions, the correlation of the modeling results for ^{18}F-FAZA and ^{15}O-H$_2$O was investigated in the musculature of the neck region (behind the cervical spine) to test the physiologic robustness of the model.

Voxelwise comparison and modeling of the compartment model and the graphical model were done using the PMOD software. The Thorwarth and Cho models were implemented using the in-house–developed software MobiTUM (version 1.0).

RESULTS

The residual activity of ^{15}O-H$_2$O ranged from 200 to 1,000 Bq/mL at the start of the ^{18}F-FAZA acquisition. After 1 h, there was around 800–2,000 Bq of ^{18}F-FAZA activity per milliliter in the blood circulation. A series of ^{18}F-FAZA images (patient 2) is shown in Figure 4.

The correlations between the kinetic features of different models for ^{18}F-FAZA and the perfusion of ^{15}O-H$_2$O flow in the tumor region are shown in Tables 2 and 3. Table 2 shows the correlation between the modeling results of ^{18}F-FAZA delivery and perfusion, and Table 3 shows the

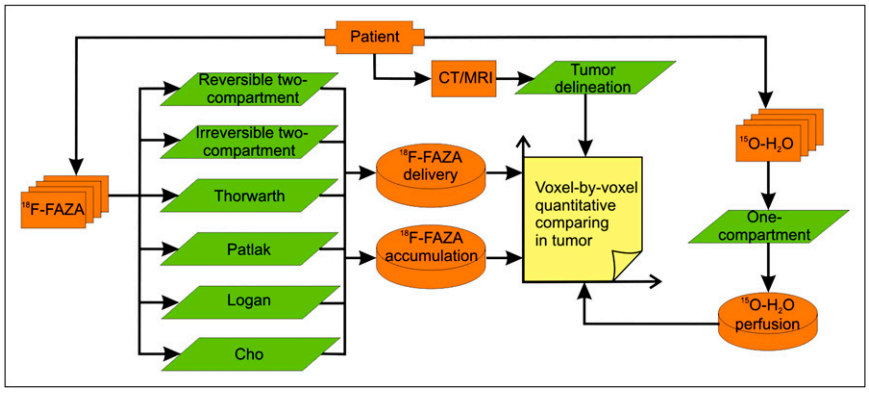

FIGURE 3. Procedure for quantitative comparison of hypoxia kinetic models.

Downloaded from jnm.snmjournals.org by on March 12, 2017. For personal use only.

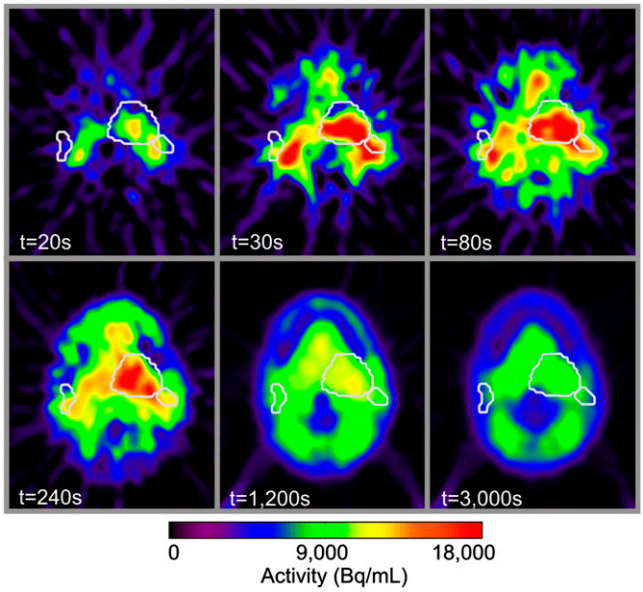

FIGURE 4. Six frames of ^{18}F-FAZA PET of a slice for patient 2. Regions of interest outline region of tumor, and *t* denotes time of start of frame.

correlation between the modeling results of the ^{18}F-FAZA accumulation and perfusion.

The Cho model shows strong positive correlations between the ^{18}F-FAZA delivery and ^{15}O-H_2O perfusion for 4 patients (patients 1–3 and 5) and a weak positive correlation for 1 patient (patient 4). Both the reversible and the irreversible 2-compartment models show positive correlations for 3 patients (patients 1, 2, and 5) and a weak positive correlation for 1 patient (patient 3). The Thorwarth model depicts positive correlations for 3 patients (patients 1, 2, and 5) and weak positive correlations for 2 patients (patients 3 and 4). Overall, the Cho model presents the strongest positive correlations among the models.

The reversible 2-compartment model shows a negative correlation between the ^{18}F-FAZA accumulation and ^{15}O-H_2O perfusion in all patients (patients 1–3, negative; patients 4 and 5, weak negative). The irreversible 2-compartment model and Cho model also show a negative correlation in 4 patients (patients 1–3, negative; patient 5, weak negative). An example of the resulting parametric images of the models (patient 2) is depicted in Figure 5. The time–activity curves of a region of interest and 2 individual pixels on the selected slice are displayed, with the corresponding fitted model curves. The voxelwise correlations between estimated ^{18}F-FAZA kinetic parameters of the reversible 2-compartment model and ^{15}O-H_2O perfusion in the tumor region for patient 2 are illustrated in Figure 6 (left side).

Kinetic models show different correlations from those shown by the static analysis (Table 1) for all patients. On average, the static assessment reveals a positive correlation between ^{18}F-FAZA accumulation and ^{15}O-H_2O perfusion, whereas the reversible and irreversible 2-compartment models and the Cho model show negative correlations between blood supply and tracer accumulation.

Different kinetic models reveal different results. Clear negative correlations between hypoxia tracer accumulation and perfusion for the reversible and the irreversible 2-compartment models and the Cho model were observed for patients 1–3. In contrast, the Thorwarth model, Patlak plot, and Logan plot revealed positive correlations for these patients.

Table 4 shows the modeling results for the correlation between the ^{18}F-FAZA delivery and ^{15}O-H_2O perfusion, and Table 5 shows the correlation between the ^{18}F-FAZA accumulation and ^{15}O-H_2O perfusion in the musculature of the neck region behind the cervical spine. A scatterplot of estimated delivery and accumulation parameters of ^{18}F-FAZA by the reversible 2-compartment model and ^{15}O-H_2O perfusion in the muscle region for patient 2 is illustrated in Figure 6. Overall, the reversible 2-compartment model shows the smallest variance considering both relations.

DISCUSSION

Using the cross-study of the kinetic modeling of the hypoxia tracer ^{18}F-FAZA and the perfusion tracer ^{15}O-H_2O, we investigated the relationship between tracer delivery and perfusion and between tracer accumulation and perfusion.

TABLE 2. Voxelwise Correlations Between ^{18}F-FAZA Delivery and Corresponding ^{15}O-H_2O Perfusion in Tumor Region for Each Patient

Patient no.	Reversible 2-compartment: K_1	Irreversible 2-compartment: K_1	Thorwarth: w_0	Cho: early
1	0.359/0.231	0.337/0.188	0.507/0.447	0.854/0.795
2	0.684/0.744	0.724/0.768	0.523/0.584	0.867/0.911
3	0.144/0.103	0.138/0.095	0.183/0.164	0.851/0.791
4	−0.025/0.003	−0.014/−0.002	0.109/0.182	0.291/0.152
5	0.352/0.349	0.332/0.326	0.372/0.388	0.694/0.705

Values after slash (/) indicate computation result when performing half-voxel shift in *x* direction for registration. Each column of table denotes 1 Pearson correlation coefficient between specified kinetic parameter of ^{18}F-FAZA modeling and kinetic parameter K_1 of ^{15}O-H_2O modeling.

Downloaded from jnm.snmjournals.org by on March 12, 2017. For personal use only.

TABLE 3. Voxelwise Correlations Between ^{18}F-FAZA Accumulation and Corresponding ^{15}O-H_2O Perfusion in Tumor Region for Each Patient

Patient no.	Reversible 2-compartment: k_3	Irreversible 2-compartment: k_3	Thorwarth: w_A	Patlak: slope	Logan: DV	Cho: late
1	−0.462/−0.356	−0.674/−0.636	0.435/0.596	0.487/0.622	0.598/0.672	−0.558/−0.647
2	−0.490/−0.499	−0.344/−0.352	0.528/0.589	0.348/0.436	0.526/0.606	−0.600/−0.627
3	−0.441/−0.428	−0.506/−0.492	0.152/0.144	0.162/0.135	0.297/0.264	−0.404/−0.326
4	−0.156/0.029	−0.094/0.087	0.578/0.637	0.556/0.641	0.416/0.548	−0.067/0.053
5	−0.107/−0.128	−0.167/−0.173	0.451/0.435	0.535/0.527	0.581/0.576	−0.242/−0.261

Values after slash (/) indicate computation result when performing half-voxel shift in *x* direction for registration. Each column of table denotes1 Pearson correlation coefficient between specified kinetic parameter of ^{18}F-FAZA modeling and kinetic parameter K_1 of ^{15}O-H_2O modeling.

Correlation Between ^{18}F-FAZA Delivery, Accumulation, and Perfusion

After the tracer (either ^{18}F-FAZA or ^{15}O-H_2O) was injected into the body, it was transported by the blood flow through the vascular system to capillaries and postcapillary venules and finally diffused into the interstitium and intracellular space, as shown in Figure 2. Because the tracer was delivered via blood flow, it was reasonable to postulate a positive correlation between drug delivery and perfusion. The results of the 4 models (the reversible and irreversible 2-compartment, Thorwarth, and Cho models) confirmed positive correlations in 4 of 5 patients (Table 2).

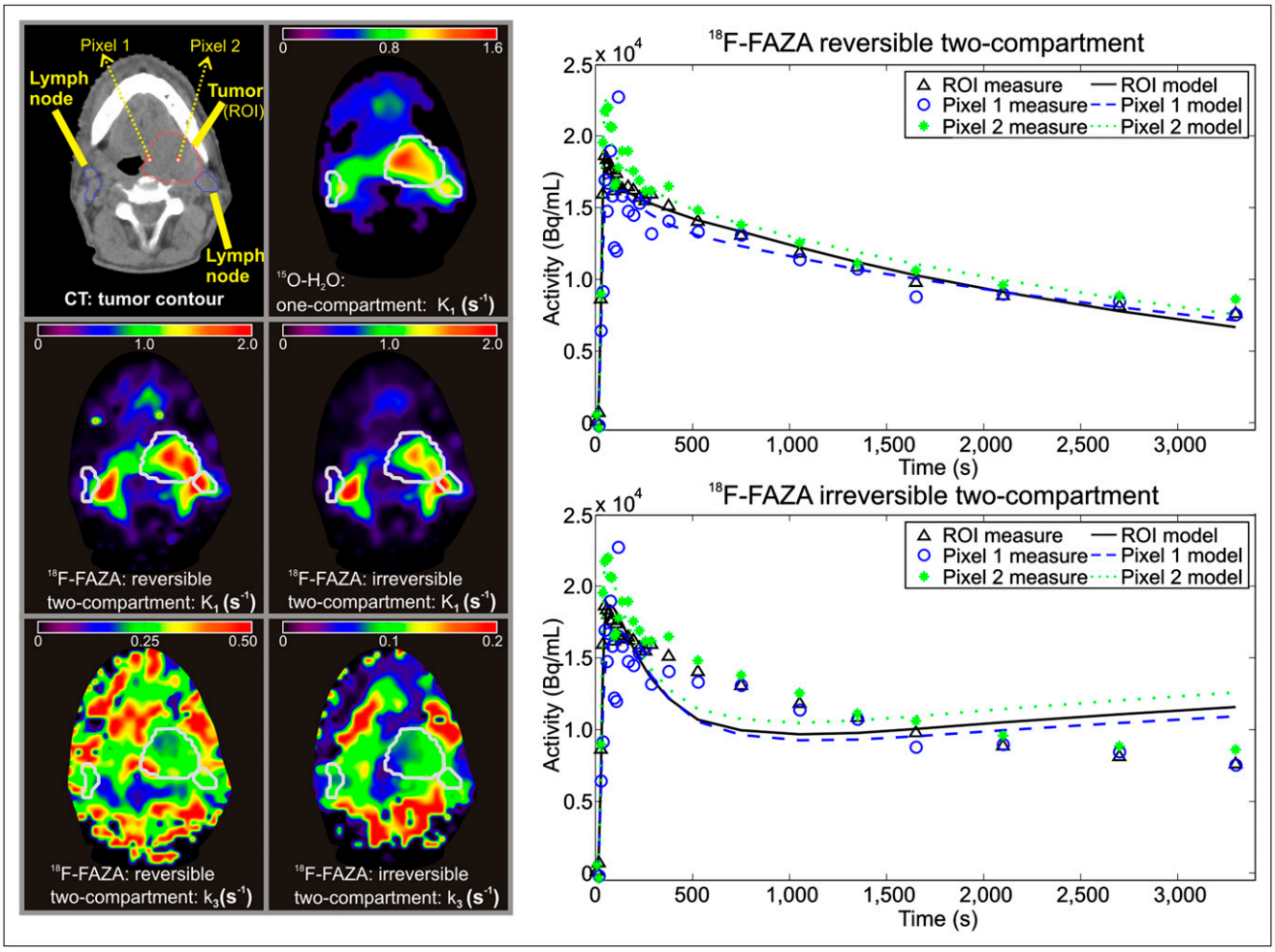

FIGURE 5. One slice of CT image and parametric images of reversible and irreversible 2-compartment models for patient 2. Parametric images are computed within region determined by CT. Time–activity curves of tumor region of interest and 2 pixels (arrows) are displayed on right, with corresponding model results. ROI = region of interest.

Downloaded from jnm.snmjournals.org by on March 12, 2017. For personal use only.

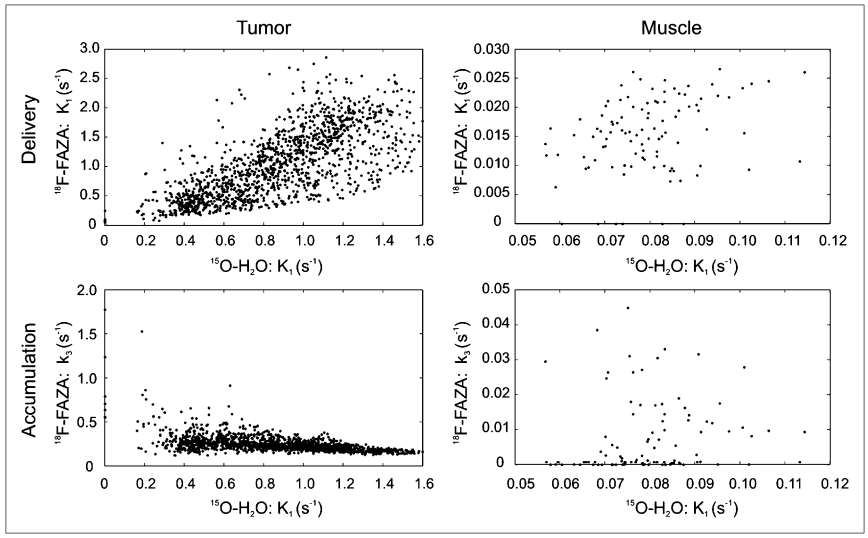

FIGURE 6. Scatterplots of voxelwise correlation between estimated parameters of reversible 2-compartment model for ^{18}F-FAZA and K_1 of 1-compartment model for ^{15}O-H_2O in tumor and muscle regions for patient 2.

The oxygenation status of tumors depends on cellular oxygen consumption and oxygen supply to the respiring cells. The latter is mainly caused by convective transport through capillaries and by diffusion from microvessels to oxygen consumption sites (*11,32,33*). A functionally disturbed microcirculation and deteriorated diffusion conditions are the primary factors of tumor hypoxia. Our hypothesis of a negative correlation between hypoxia and perfusion is based on this fact. The results from the reversible and irreversible 2-compartment models and the Cho model support this hypothesis in 4 of 5 patients (Table 3). Although the Thorwarth model is based on the irreversible 2-compartment model, it recombines the fittable parameters of the irreversible 2-compartment model. Supposing an ideal fit by these 2 models yielding the same model curve, the parameter w_A in the Thorwarth model equals the product of K_1 and $k_3/(k_2 + k_3)$ in the irreversible 2-compartment model. Thus, the Thorwarth model is not able to uncover the negative correlation between ^{18}F-FAZA and ^{15}O-H_2O perfusion. Similarly, the graphical models yield mixed kinetics and cannot discriminate the negative correlation and lead to opposite results.

For patient 4, no clear correlation was observed between ^{18}F-FAZA delivery or accumulation and blood perfusion for the reversible and irreversible 2-compartment models and Cho model. The ^{18}F-FAZA uptake is influenced by the existence of acute hypoxia (*34*). The intensity of ^{18}F-FAZA in a PET voxel represents the mixed uptake of tumor microenvironment (*34*). The uptake varies on a microscopic scale, even within the same acquisition duration including morphologic and functional abnormalities of blood vessels (*11*), red blood cell fluxes (*35*), and dynamics of tumor hypoxia (*36,37*). Besides, although ^{18}F-FAZA is an effective hypoxia tracer, it still has difficulty reaching all hypoxic areas distant from tumor microvessels (*20*).

Physiology Consistency of Normal Skeletal Muscle

In our study, we analyzed both the ^{15}O-H_2O and the ^{18}F-FAZA dynamic uptake for normal musculature of the neck region (behind the cervical spine), which are skeletal muscles preferentially containing type I fibers (high capillary density, high oxidative capacity, and low glycolytic activity) (*38*). Muscle fibers and blood capillaries are usually uniformly structured (*38*). Our measurements were performed on resting muscles. Therefore, it is reasonable to assume that they have a consistent physiology and thus coherent tracer kinetics for ^{15}O-H_2O and ^{18}F-FAZA. On the basis of this assumption, the observed variance in the

TABLE 4. Voxelwise Correlations Between ^{18}F-FAZA Delivery and Corresponding ^{15}O-H_2O Perfusion in Region of Muscle for Each Patient

Patient no.	Reversible 2-compartment: K_1	Irreversible 2-compartment: K_1	Thorwarth: w_0	Cho: early
1	0.412	0.344	−0.131	0.436
2	0.230	0.112	−0.068	0.320
3	0.888	0.929	0.414	0.931
4	0.598	0.682	0.117	0.720
5	0.349	0.182	−0.066	0.046
σ	0.257	0.347	0.222	0.345

Each column of table denotes 1 Pearson correlation coefficient between specified kinetic parameter of ^{18}F-FAZA modeling and kinetic parameter K_1 of ^{15}O-H_2O modeling. σ is SD of normalized correlations of all patients in column.

Downloaded from jnm.snmjournals.org by on March 12, 2017. For personal use only.

TABLE 5. Voxelwise Correlations Between ^{18}F-FAZA Accumulation and Corresponding ^{15}O-H_2O Perfusion in Region of Muscle for Each Patient

Patient no.	Reversible 2-compartment: k_3	Irreversible 2-compartment: k_3	Thorwarth: w_A	Patlak: slope	Logan: DV	Cho: late
1	0.166	0.087	0.114	0.226	0.143	−0.290
2	0.111	−0.176	0.476	0.491	0.343	−0.065
3	−0.379	0.567	0.868	0.862	0.351	−0.814
4	0.281	0.446	0.674	0.792	0.309	−0.667
5	0.232	0.050	−0.094	−0.068	−0.300	−0.239
σ	0.266	0.305	0.396	0.389	0.276	0.313

Each column of table denotes 1 Pearson correlation coefficient between specified kinetic parameter of ^{18}F-FAZA modeling and kinetic parameter K_1 of ^{15}O-H_2O modeling. σ is SD of normalized correlations of all patients in column.

correlations between ^{15}O-H_2O and ^{18}F-FAZA modelings should be due to the poor physiologic robustness of the models. However, this variation may also be due to muscle activities, such as that caused by emotional stress (*39*).

Physiologic Precision and Mathematic Accuracy

The physiologic precision and numeric accuracy are 2 sides of kinetic modeling. An increase in model complexity can improve the ability of physiologic description and enhance the understanding of multifaceted mechanisms. However, this increase may decrease the accuracy of mathematic computation and lead to instability of quantitative assessment.

In our study, the reversible 2-compartment model has smaller physiologic variance for normal muscle; thus, it is more physiologically robust. However, the 2-compartment model had mathematic instability during the optimization procedure, which is not found for the graphical and Cho models.

Nonlinear optimization in voxelwise fitting (reversible and irreversible 2-compartment models, Thorwarth model) is sensitive to noise. Even using the gaussian convolution, it is still possible to see singularities in parametric images (Fig. 5). However, in the outlined tumor regions, the fitting result is relatively continuous. One additional initial setting of doubled magnitude was tested for patients 2 and 4, and the influence of the initial values on the correlations was observed. Slight changes below 5% in the resulting correlations were observed, except for patient 4, for whom the correlation between K_1 of the irreversible 2-compartment model and ^{15}O-H_2O perfusion changed from −0.014 (in Table 2) to −0.004. Despite this, the characteristics of the correlations remained unchanged for all patients.

Although an immobilization mask was continuously used during the whole study, uncertainty (<2 mm) may still exist in spatial registration of the sequential ^{18}F-FAZA and ^{15}O-H_2O PET images because of motion during the long acquisition (*34*). This may compromise the voxel-by-voxel correlation analysis. The influence of this registration uncertainty was tested by applying a half-voxel shift in the x direction to the registration between the ^{18}F-FAZA and ^{15}O-H_2O images (Tables 2 and 3). The resulting voxelwise correlation was affected by the alignment of the images, especially for low correlations. However, the characteristics of the investigated correlations were not changed within the accuracy range of this study.

Furthermore, we have not evaluated the 1-compartment model for ^{15}O-H_2O perfusion (*6*), because our purpose was to compare only the hypoxia kinetic models.

Our results suggest that consideration of both the precise physiologic background and the mathematic accuracy is needed for a successful modeling of tumor hypoxia.

Our feasibility study is limited by the small number of patients because our imaging protocol is complex. Nevertheless, we proved the possibilities of physiologically assessing mathematic models with clinical relevance, achieved by a cross-study of correlated biologic characteristics, which can be tracked through molecular imaging techniques.

CONCLUSION

Although kinetic modeling has advantages over static assessment (*21*), the behavior varies greatly for different models of hypoxia evaluation. Different models even lead to opposite interpretations in some situations. According to our criteria for physiologic precision and robustness assessment, preference should be given to the reversible 2-compartment model.

Although only positive or negative relations were considered here, concrete quantitative knowledge of the correlations is important for the definition of more reliable evaluation criteria. The dilemma of physiologic precision and mathematic accuracy requires a thorough investigation of both tumor pathophysiology and mathematic models before the application of kinetic analysis. A large clinical study is desired for further model assessment. Theoretic simulation is another way to improve the understanding of kinetic modeling and the underlying physiology.

ACKNOWLEDGMENTS

We thank Professors Michael Molls and Markus Schwaiger for their valuable discussion and support. The detailed discussions with Dr. Daniela Thorwarth on modeling approaches are highly appreciated. Furthermore, we thank

Downloaded from jnm.snmjournals.org by on March 12, 2017. For personal use only.

Isabella Miederer for her input concerning data analysis. The excellent technical assistance of Gitti Dzewas in performing the PET studies is greatly acknowledged. We also thank Dr. Christine Bayer for the linguistic refinement. This work was supported in part by the DFG grant WE 2386/4-2, BMBF MobiTUM project (01EZ0826), and DFG Cluster of Excellence: Munich-Centre for Advanced Photonics. Part of this work was presented at the IEEE Nuclear Science Symposium and Medical Imaging Conference in Orlando, Florida, October 25–31, 2009.

REFERENCES

1. Huang SC, Phelps ME. Principles of tracer kinetic modeling in positron emission tomography and autoradiography. In: Phelps ME, Mazziotta J, Schelbert HR, eds. *Positron Emission Tomography and Autoradiography: Principles and Applications for the Brain and Heart*. New York, NY: Raven Press; 1986:287–346.
2. Gunn RN, Gunn SR, Cunningham VJ. Positron emission tomography compartmental models. *J Cereb Blood Flow Metab*. 2001;21:635–652.
3. Lammertsma AA, Hume SP. Simplified reference tissue model for PET receptor studies. *Neuroimage*. 1996;4:153–158.
4. Patlak CS, Blasberg RG, Fenstermacher JD. Graphical evaluation of blood-to-brain transfer constants from multiple-time uptake data. *J Cereb Blood Flow Metab*. 1983;3:1–7.
5. Logan J, Fowler JS, Volkow ND, et al. Graphical analysis of reversible radioligand binding from time-activity measurements applied to [*N*-^{11}C-methyl]-(−)-cocaine PET studies in human subjects. *J Cereb Blood Flow Metab*. 1990;10:740–747.
6. Choi Y, Huang SC, Hawkins RA, et al. Quantification of myocardial blood flow using ^{13}N-ammonia and PET: comparison of tracer models. *J Nucl Med*. 1999;40:1045–1055.
7. Kropholler MA, Boellaard R, Schuitemaker A, Folkersma H, Berckel BNM, Lammertsma AA. Evaluation of reference tissue models for the analysis of [lsqb]^{11}C[rsqb](*R*)-PK11195 studies. *J Cereb Blood Flow Metab*. 2006;26:1431–1441.
8. Feng D, Ho D, Chen K, et al. An evaluation of the algorithms for determining local cerebral metabolic rates of glucose using positron emission tomography dynamic data. *IEEE Trans Med Imaging*. 1995;14:697–710.
9. Yaqub M, Boellaard R, Kropholler MA, Lammertsma AA. Optimization algorithms and weighting factors for analysis of dynamic PET studies. *Phys Med Biol*. 2006;51:4217–4232.
10. Wang W, Georgi JC, Nehmeh SA, et al. Evaluation of a compartmental model for estimating tumor hypoxia via FMISO dynamic PET imaging. *Phys Med Biol*. 2009;54:3083–3099.
11. Vaupel P, Kallinowski F, Okunieff P. Blood flow, oxygen and nutrient supply, and metabolic microenvironment of human tumors: a review. *Cancer Res*. 1989;49:6449–6465.
12. Vaupel P, Schlenger K, Knoop C, Höckel M. Oxygenation of human tumors: evaluation of tissue oxygen distribution in breast cancers by computerized O_2 tension measurements. *Cancer Res*. 1991;51:3316–3322.
13. Padhani AR, Krohn KA, Lewis JS, Alber M. Imaging oxygenation of human tumours. *Eur Radiol*. 2007;17:861–872.
14. Koh WJ, Rasey JS, Evans ML, et al. Imaging of hypoxia in human tumors with ^{18}FFluoromisonidazole. *Int J Radiat Oncol Biol Phys*. 1992;22:199–212.
15. Rasey JS, Koh WJ, Evans ML, et al. Quantifying regional hypoxia in human tumors with positron emission tomography of ^{18}F-fluoromisonidazole: a pretherapy study of 37 patients. *Int J Radiat Oncol Biol Phys*. 1996;36:417–428.
16. Lehtio K, Eskola O, Viljanen T, et al. Imaging perfusion and hypoxia with PET to predict radiotherapy response in head-and-neck cancer. *Int J Radiat Oncol Biol Phys*. 2004;59:971–982.
17. Lewis JS, Herrero P, Sharp TL, et al. Delineation of hypoxia in canine myocardium using PET and copper(II)-diacetyl-bis(*N*4-methylthiosemicarbazone). *J Nucl Med*. 2002;43:1557–1569.
18. Piert M, Machulla HJ, Picchio M, et al. Hypoxia-specific tumor imaging with ^{18}F-fluoroazomycin arabinoside. *J Nucl Med*. 2005;46:106–113.
19. Souvatzoglou M, Grosu AL, Röper B, et al. Tumour hypoxia imaging with ^{18}F-FAZA PET in head and neck cancer patients: a pilot study. *Eur J Nucl Med Mol Imaging*. 2007;34:1566–1575.
20. Minchinton AI, Tannock IF. Drug penetration in solid tumours. *Nat Rev Cancer*. 2006;6:583–592.
21. Thorwarth D, Eschmann SM, Paulsen F, Alber M. A kinetic model for dynamic ^{18}FFmiso PET data to analyse tumour hypoxia. *Phys Med Biol*. 2005;50:2209–2224.
22. Casciari JJ, Graham MM, Rasey JS. A modeling approach for quantifying tumor hypoxia with ^{18}F-fluoromisonidazole PET time-activity data. *Med Phys*. 1995;22:1127–1139.
23. Cho H, Ackerstaff E, Carlin S, et al. Noninvasive multimodality imaging of the tumor microenvironment: registered dynamic magnetic resonance imaging and positron emission tomography studies of a preclinical tumor model of tumor hypoxia. *Neoplasia*. 2009;11:247–259.
24. Busk M, Horsman M, Jakobsen S, et al. Imaging hypoxia in xenografted and murine tumors with ^{18}F-fluoroazomycin arabinoside: a comparative study involving microPET, autoradiography, pO_2-polarography, and fluorescence microscopy. *Int J Radiat Oncol Biol Phys*. 2008;70:1202–1212.
25. Carlin S, Pugachev A, Sun X, et al. In vivo characterization of a reporter gene system for imaging hypoxia-induced gene expression. *Nucl Med Biol*. 2009;36:821–831.
26. Lehtio K, Oikonen V, Gronroos T, et al. Imaging of blood flow and hypoxia in head and neck cancer: initial evaluation with ^{15}O-H_2O and ^{18}F-fluoroerythronitroimidazole PET. *J Nucl Med*. 2001;42:1643–1652.
27. Bruehlmeier M, Roelcke U, Schubiger PA, Ametamey SM. Assessment of hypoxia and perfusion in human brain tumors using PET with ^{18}F-fluoromisonidazole and ^{15}O-H_2O. *J Nucl Med*. 2004;45:1851–1859.
28. Iida H, Miura S, Shoji Y, et al. Noninvasive quantitation of cerebral blood flow using oxygen-15-water and a dual-PET system. *J Nucl Med*. 1998;39:1789–1798.
29. Feng D, Huang SC, Wang X. Models for computer simulation studies of input functions for tracer kinetic modeling with positron emission tomography. *Int J Biomed Comput*. 1993;32:95–110.
30. de Langen AJ, Lubberink M, Boellaard R, et al. Reproducibility of tumor perfusion measurements using ^{15}O-labeled water and PET. *J Nucl Med*. 2008;49:1763–1768.
31. Bruehlmeier M, Kaser-Hotz B, Achermann R, et al. Measurement of tumor hypoxia in spontaneous canine sarcomas. *Vet Radiol Ultrasound*. 2005;46:348–354.
32. Höckel M, Vaupel P. Tumor hypoxia: definitions and current clinical, biologic, and molecular aspects. *J Natl Cancer Inst*. 2001;93:266–276.
33. Vaupel P, Höckel M, Mayer A. Detection and characterization of tumor hypoxia using pO2 histography. *Antioxid Redox Signal*. 2007;9:1221–1236.
34. Wang K, Yorke E, Nehmeh SA, Humm JL, Ling CC. Modeling acute and chronic hypoxia using serial images of ^{18}F-FMISO PET. *Med Phys*. 2009;36:4400–4408.
35. Kimura H, Braun RD, Ong ET, et al. Fluctuations in red cell flux in tumor microvessels can lead to transient hypoxia and reoxygenation in tumor parenchyma. *Cancer Res*. 1996;56:5522–5528.
36. Vaupel P. Pathophysiology of solid tumors. In: Molls M, Vaupel P, Nieder C, Anscher MS, eds. *The Impact of Tumor Biology on Cancer Treatment and Multidisciplinary Strategies*. Berlin, Heidelberg, Germany: Springer; 2009:51–92.
37. Vaupel P. Physiological mechanisms of treatment resistance. In: Molls M, Vaupel P, Nieder C, Anscher MS, eds. *The Impact of Tumor Biology on Cancer Treatment and Multidisciplinary Strategies*. Berlin, Heidelberg, Germany: Springer; 2009:273–290.
38. Thews G, Mutschler E, Vaupel P. *Anatomie, Physiologie, Pathophysiologie des Menschen*. 6th ed. Stuttgart, Germany: Wissenschaftliche Verlagsgesellschaft; 2007.
39. Ruotsalainen U, Raitakari M, Nuutila P, et al. Quantitative blood flow measurement of skeletal muscle using oxygen-15-water and PET. *J Nucl Med*. 1997;38:314–319.

Downloaded from jnm.snmjournals.org by on March 12, 2017. For personal use only.

JNM The Journal of NUCLEAR MEDICINE

Quantitative Assessment of Hypoxia Kinetic Models by a Cross-Study of Dynamic ^{18}F-FAZA and ^{15}O-H_2O in Patients with Head and Neck Tumors

Kuangyu Shi, Michael Souvatzoglou, Sabrina T. Astner, Peter Vaupel, Fridtjof Nüsslin, Jan J. Wilkens and Sibylle I. Ziegler

J Nucl Med. 2010;51:1386-1394.
Published online: August 18, 2010.
Doi: 10.2967/jnumed.109.074336

This article and updated information are available at:
http://jnm.snmjournals.org/content/51/9/1386

Information about reproducing figures, tables, or other portions of this article can be found online at:
http://jnm.snmjournals.org/site/misc/permission.xhtml

Information about subscriptions to JNM can be found at:
http://jnm.snmjournals.org/site/subscriptions/online.xhtml

The Journal of Nuclear Medicine is published monthly.
SNMMI | Society of Nuclear Medicine and Molecular Imaging
1850 Samuel Morse Drive, Reston, VA 20190.
(Print ISSN: 0161-5505, Online ISSN: 2159-662X)

© Copyright 2010 SNMMI; all rights reserved.

SNMMI SOCIETY OF NUCLEAR MEDICINE AND MOLECULAR IMAGING